Three-Dimensional Green's Functions in Anisotropic Elastic Bimaterials With Imperfect Interfaces

E. Pan[1]
Structures Technology, Inc.,
543 Keisler Drive, Suite 204,
Cary, NC 27511
Mem. ASME

In this paper, three-dimensional Green's functions in anisotropic elastic bimaterials with imperfect interface conditions are derived based on the extended Stroh formalism and the Mindlin's superposition method. Four different interface models are considered: perfect-bond, smooth-bond, dislocation-like, and force-like. While the first one is for a perfect interface, other three models are for imperfect ones. By introducing certain modified eigenmatrices, it is shown that the bimaterial Green's functions for the three imperfect interface conditions have mathematically similar concise expressions as those for the perfect-bond interface. That is, the physical-domain bimaterial Green's functions can be obtained as a sum of a homogeneous full-space Green's function in an explicit form and a complementary part in terms of simple line-integrals over [0,π] suitable for standard numerical integration. Furthermore, the corresponding two-dimensional bimaterial Green's functions have been also derived analytically for the three imperfect interface conditions. Based on the bimaterial Green's functions, the effects of different interface conditions on the displacement and stress fields are discussed. It is shown that only the complementary part of the solution contributes to the difference of the displacement and stress fields due to different interface conditions. Numerical examples are given for the Green's functions in the bimaterials made of two anisotropic half-spaces. It is observed that different interface conditions can produce substantially different results for some Green's stress components in the vicinity of the interface, which should be of great interest to the design of interface. Finally, we remark that these bimaterial Green's functions can be implemented into the boundary integral formulation for the analysis of layered structures where imperfect bond may exist. [DOI: 10.1115/1.1546243]

Introduction

Interface modeling has been the subject of numerous studies in material science and composite structure. The importance of researches in this topic cannot be overemphasized as it is directly related to the prediction of the overall material properties, delamination, transmission of force, etc. (see, e.g., [1–13]). The most ideal interface model, as is well known, is the so-called perfect-bond interface where the displacements and tractions are continuous across the interface. However, interfaces are seldom perfect, and therefore various imperfect models have been introduced, such as the three-phase and linear spring-like models (see, i.e., [14–16]). Although these models are more capable of representing the imperfect interface, the associated Green's functions are very difficult to derive ([14–17]). Perhaps the most frequently studied imperfect interface model is the smooth-bond interface where the normal components of the displacement and traction are continuous across the interface while the shear traction components are zero on the interface from both sides of the bimaterials (see, e.g., [1,2,18]). This model is much simpler than the three-phase and linear spring-like models, and has been used to describe the connection between two materials at elevated temperature ([17]), and to model the bone implants in biomechanics ([19]). Recently, Shuvalov and Gorkunova [18] studied the corresponding wave propagation in anisotropic bimaterials with smooth-bond interface where they found certain special features associated with the smooth-bond interface. Besides various homogeneous interface models mentioned above, Ru [20,21] has recently proposed an inhomogeneously imperfect interface model where the interface parameters are functions of the position variable along the interface, instead of constants along the whole interface for the homogeneous case.

While various interface-related studies have been carried out for two-dimensional deformation problems, relatively very few literatures are available for the corresponding three-dimensional deformations, especially with a planar interface. An apparent reason is that most three-dimensional problems are complicated and need to be solved numerically. Since singular stress field is usually associated with problems involving interface, a more suitable numerical tool would be the boundary integral equation method (i.e., [22]). However, successful application of the boundary integral equation method depends upon the variability of the related Green's functions. Unfortunately, as far as the three-dimensional bimaterial Green's functions with imperfect interface are concerned, only those with the smooth-bond interface for isotropic [1,23,24]) and transversely isotropic ([25]) materials were obtained previously. More recently, Yu [14] introduced a dislocation-like model where the interface condition is similar to the linear spring-like model but with the displacement on one side of the interface being assumed to be linearly proportional to that on the other side of the interface. This dislocation-like model enjoys at least two advantages: (1) The interface shear stress predicted by this model agreed qualitatively with experimental measurements ([15]), a suitable description on the effect of an imperfect interface

[1]Currently at the Department of Civil Engineering, University of Akron, Akron, OH 44325-3905. e-mail: pan2@uakron.edu

Contributed by the Applied Mechanics Division of THE AMERICAN SOCIETY OF MECHANICAL ENGINEERS for publication in the ASME JOURNAL OF APPLIED MECHANICS. Manuscript received by the ASME Applied Mechanics Division, May 8, 2001; final revision, Mar. 5, 2002. Associate Editor: D. A. Kouris. Discussion on the paper should be addressed to the Editor, Prof. Robert M. McMeeking, Department of Mechanical and Environmental Engineering University of California–Santa Barbara, Santa Barbara, CA 93106-5070, and will be accepted until four months after final publication of the paper itself in the ASME JOURNAL OF APPLIED MECHANICS.

on the load transfer and (2) For this model, the exact closed-form bimaterial Green's functions can be derived ([14,15]).

Besides their application as kernel functions in the boundary integral equation method, the three-dimensional Green's functions, in particular, the three-dimensional bimaterial Green's functions with various interface conditions, are of special values in the numerical studies of strained semiconductor quantum devices where the strain-induced quantum dot growth in semiconductor nanostructures is crucial to the electronic performance ([26–28]). While under two-dimensional deformation, the strain-induced elastic fields can be easily analyzed using the analytical solution ([29]), for those in the three-dimensional bimaterial space, the Green's functions, as embedded in the Eshelby tensor ([30,31]), are required in the corresponding studies. Unfortunately, for problems with material anisotropy, as for the strained semiconductor quantum devices, the involved three-dimensional Green's functions are very difficult to derive.

In recent years, the Stroh formalism, originally developed by Stroh ([32,33]) for the two-dimensional deformation problems, has been extended to certain three-dimensional Green's function solutions ([34–37]). This opens a new door to further exploring the Stroh formalism. The most promising feature, perhaps, is the application of the extended three-dimensional Stroh formalism combined with the Mindlin's superposition method ([38]), as in Pan and Yuan [37]. In doing so, the three-dimensional bimaterial Green's functions can be expressed as a sum of the Kelvin solution (the full-space Green's function) and a Mindlin's complimentary part ([37]). While the former has an explicit expression ([39–42]), the latter is expressed in terms of a simple and regular line integral over $[0,\pi]$. This is perhaps the most simple and concise approach available since a direct application of the Fourier transform would end up with a Green's function expression in terms of three-dimensional Fourier integrals for the homogeneous full-space and four-dimensional Fourier integrals for the bimaterial full-space ([43]).

In this paper, we further extend the three-dimensional Stroh formalism and Mindlin's superposition method to the study of the three-dimensional Green's functions in anisotropic elastic bimaterials with imperfect interface. Four different interface models, namely perfect-bond, smooth-bond, dislocation-like, and force-like, are considered. While the first model is for a perfect interface for which the corresponding bimaterial Green's functions were derived by Pan and Yuan [37], other three models are for imperfect interfaces for which the corresponding bimaterial Green's functions are derived in this paper. Furthermore, the dislocation-like model has been generalized by introducing an interface spring-like matrix, instead of only two parameters, and the force-like model is a complete new one resembling the recently proposed traction-jump model ([16,44,45]) with its potential application yet to be found. We will show that even for the three imperfect interface models, the bimaterial Green's functions can still enjoy the same simple and concise structure as that for the perfect interface model. This is actually achieved by carefully introducing certain modified eigenmatrices corresponding to the imperfect interface conditions. We also remark that while the generalized Mindlin's problem in an anisotropic elastic half-space with general boundary conditions has been recently solved by the author ([46]), the corresponding two-dimensional bimaterial Green's functions with the three imperfect interface models are derived analytically in the Appendix of this paper.

A typical numerical example on the Green's stress distribution is given for a bimaterial full-space made of two orthotropic half-spaces with the four different interface models. It is demonstrated clearly that by varying the interface parameters in the dislocation-like and force-like models, various load transfer states can be simulated. It is observed that, for most Green's stresses, the four different interface models affect only their local distribution behaviors in the vicinity of the interface, and that among the three imperfect interface models, the smooth-bond model shows the greatest variation as compared to the perfect-bond results. These features should be of great interest to the composite structure analysis, in particular, to the interface design. Since the bimaterial Green's functions for the four interface conditions can be obtained very efficiently and accurately, they can also be implemented into a boundary integral formulation to investigate the deformation, stress, and fracture problems in anisotropic and layered structures with imperfect interfaces.

Problem Description

Consider an anisotropic elastic bimaterial full-space where $x_3>0$ and $x_3<0$ are occupied, respectively, by materials 1 and 2 with interface at $x_3=0$ plane. Without loss of generality, we assume that a point force $\mathbf{f}=(f_1,f_2,f_3)$ is applied in material 1 at source point $\mathbf{d}\equiv(d_1,d_2,d_3\equiv d>0)$, with the field point being denoted by $\mathbf{x}\equiv(x_1,x_2,x_3\equiv z)$[2]. Following Pan and Yuan [36], the problem domain is now artificially divided into three regions: $z>d$ (in material 1), $0\leqslant z<d$ (in material 1), and $z<0$ (in material 2).

Since each region is now free of the body force, the equation of equilibrium in terms of the elastic displacements u_k can thus be written as

$$C_{ijkl}u_{k,lj}=0 \tag{1}$$

where C_{ijkl} is the elastic stiffness tensor of the corresponding region. As a convention, summation is taken for the repeated index from 1 to 3, and an index following the subscript comma denotes the partial differentiation with respect to the field coordinate.

Equation (1) needs to be solved for each region with suitable continuity conditions along the interface and at the source level. In this paper, four different interface models are considered, with one being perfect and three being imperfect.

Model 1. The displacement and traction vectors are continuous across the interface, i.e.,

$$u_j^{(1)}|_{z=0^+}=u_j^{(2)}|_{z=0^-},\quad t_j^{(1)}|_{z=0^+}=t_j^{(2)}|_{z=0^-};\quad j=1,2,3 \tag{2a}$$

where the superscripts (1) and (2) are used exclusively to denote the quantities in materials 1 and 2, respectively. It is seen that, for this model, the two half-spaces are perfectly bonded together, and such an interface is also called perfect-bond (or ideal, welded) interface (see, e.g., [1,17,24]). We further mention that the anisotropic bimaterial Green's functions with this interface condition have been derived recently by Pan and Yuan [37] and are included here for the purpose of comparison to the bimaterial Green's functions with imperfect interface conditions.

Model 2. The displacement and traction vectors are required to satisfy the following conditions across the interface:

$$\begin{gathered} u_3^{(1)}|_{z=0^+}=u_3^{(2)}|_{z=0^-},\quad t_3^{(1)}|_{z=0^+}=t_3^{(2)}|_{z=0^-} \\ t_\alpha^{(1)}|_{z=0^+}=t_\alpha^{(2)}|_{z=0^-}=0,\quad \alpha=1,2. \end{gathered} \tag{2b}$$

This is perhaps one of the most frequently studied imperfect interface models and is called smooth-bond (or frictionless, slipping, or sliding) interface ([1,17,24,25]).

Model 3. Across the interface, the traction vector is continuous and the displacement vector is discontinuous:

$$u_i^{(1)}|_{z=0^+}=k_{ij}^u u_j^{(2)}|_{z=0^-},\quad t_i^{(1)}|_{z=0^+}=t_i^{(2)}|_{z=0^-};\quad i=1,2,3 \tag{2c}$$

where the constant matrix $\mathbf{k}^u=[k_{ij}^u]$ describes the bonding condition along the interface. Yu ([14]) recently proposed this imperfect interface model for the isotropic bimaterial full-space with the

[2]Thereafter, the scalar variables z and d will be used exclusively for the third field coordinate x_3 and third source coordinate d_3, respectively.

constant matrix $\mathbf{k}^u$ being diagonal. This new model is called dislocation-like because of its similarity to the Somigliana's dislocation ([31]). Yu [14] proved that for this new interface model, the three-dimensional isotropic bimaterial Green's function possesses the same simple structure as that for the perfect-bond model, and that the load transfer at the interface predicted with this model is quantitatively comparable to the experimental measurement. Furthermore, two special cases can be reduced from this model: (a) If k_{ij}^u is an identity matrix, implying vanishing of the displacement jumps at the interface, the dislocation-like model is then reduced to Model 1, i.e., the perfect-bond interface and (b) if k_{ij}^u is a zero matrix, then the bimaterial problem is reduced to two separate half-space problems. With a point force being applied in material 1, the half-space problem for material 1 can be first solved subject to a rigid surface boundary condition (i.e., the surface displacements are zero). Then, the solution in the half-space of material 2 can be solved using the traction surface condition of Eq. (2*c*). Therefore, with the element values of the matrix k_{ij}^u varying from 0 (for rigid-bond) to 1 (for perfect-bond), the dislocation-like model can actually simulate various intermediate interface conditions between these two extreme cases. Another interesting feature associated with this model is that when the matrix k_{ij}^u is diagonal, the first two elements on the diagonal are related to the interface conditions in the tangential directions and the third one to the condition in the normal direction of the interface. In the following analysis, we assume that the matrix k_{ij}^u is diagonal with values in the interval (0,1) and that its inverse exists.

Model 4. In contrast with Model 3, here across the interface, the displacement vector is continuous while the traction vector is discontinuous:

$$u_i^{(1)}|_{z=0^+}=u_i^{(2)}|_{z=0^-},\quad t_i^{(1)}|_{z=0^+}=k_{ij}^t t_j^{(2)}|_{z=0^-};\quad i=1,2,3. \tag{2d}$$

Similarly, the constant matrix $\mathbf{k}^t=[k_{ij}^t]$ describes the bonding condition along the interface. This new model, being named as force-like model, describes a traction jump at the interface. We remark that this force-like model resembles the traction-jump model proposed recently by Benveniste [16], Benveniste and Chen [44], and Hashin [45] and that it includes two previous models as its special cases: (a) If k_{ij}^t is an identity matrix, implying vanishing of the traction jumps at the interface, the force-like model is then reduced to Model 1, i.e., the perfect-bond interface; and (b) if k_{ij}^t is a zero matrix, then the bimaterial problem is reduced to two separate half-space problems. With a point force being applied in material 1, the half-space problem for material 1 can be first solved subject to a traction-free surface boundary condition. Then, the solution in the half-space of material 2 can be derived using the displacement surface condition of Eq. (2*d*). Consequently, with the element values of the matrix k_{ij}^t varying from 0 (traction-free) to 1 (perfect-bond), the force-like model can actually be used to simulate the load transfer along various intermediate interfaces between these two extreme cases. Furthermore, similar to Model 3, if the matrix k_{ij}^t is diagonal, then the first two elements on the diagonal are related to the interface conditions in the tangential directions and the third one to the condition in the normal direction of the interface. Again, we assume that the inverse of the matrix k_{ij}^t exists.

Besides the interface conditions at $z=0$, one will also need the condition at the source level in order to solve the bimaterial Green's functions. It is found that, at the source level $z=d$ where the point force is applied, the displacement and traction vectors are required to satisfy the following conditions:

$$\begin{aligned}\mathbf{u}^{(1)}|_{z=d^-}&=\mathbf{u}^{(1)}|_{z=d^+}\\ \mathbf{t}^{(1)}|_{z=d^-}-\mathbf{t}^{(1)}|_{z=d^+}&=\delta(x_1-d_1)\,\delta(x_2-d_2)\mathbf{f}\end{aligned} \tag{3}$$

where the displacement and traction vectors $\mathbf{u}$ and $\mathbf{t}$ are defined as

$$\begin{aligned}\mathbf{u}&=(u_1,u_2,u_3)\\ \mathbf{t}&\equiv(\sigma_{13},\sigma_{23},\sigma_{33})\equiv(t_1,t_2,t_3).\end{aligned} \tag{4}$$

Finally, the Green's function solutions are required to vanish as $|\mathbf{x}|$ approaches infinity.

Bimaterial Green's Functions in the Transformed Domain

To solve the problem described in the previous section, the two-dimensional Fourier transform, i.e., for the displacement,

$$\tilde{u}_k(y_1,y_2,z;\mathbf{d})=\int\int u_k(x_1,x_2,z;\mathbf{d})e^{iy_\alpha x_\alpha}dx_1dx_2 \tag{5}$$

is applied to Eq. (1) for the three regions. In Eq. (5), α takes the summation from 1 to 2. We point out that, when carrying out the double Fourier inverse transforms later on, a polar coordinate system that relates the Fourier variables (y_1,y_2) as

$$y_1=\eta\cos\theta;\quad y_2=\eta\sin\theta \tag{6}$$

will be used, [37].

Applying the two-dimensional Fourier transform to the continuity conditions (2*a*–*d*) at the interface $z=0$ and the condition (3) at the source level $z=d$, the general solution in the transformed domain that satisfies the source level condition can be expressed in terms of the Stroh eigenvalues and the corresponding eigenmatrices as ([34,37]):

For $z>d$ (in material 1):

$$\begin{aligned}\tilde{\mathbf{u}}^{(1)}(y_1,y_2,z;\mathbf{d})&=-i\eta^{-1}\overline{\mathbf{A}}^{(1)}\langle e^{-i\overline{p}_*^{(1)}\eta(z-d)}\rangle\overline{\mathbf{q}}^{\infty}-i\eta^{-1}\overline{\mathbf{A}}^{(1)}\\ &\quad\times\langle e^{-i\overline{p}_*^{(1)}\eta z}\rangle\overline{\mathbf{q}}^{(1)}\\ \tilde{\mathbf{t}}^{(1)}(y_1,y_2,z;\mathbf{d})&=-\overline{\mathbf{B}}^{(1)}\langle e^{-i\overline{p}_*^{(1)}\eta(z-d)}\rangle\overline{\mathbf{q}}^{\infty}-\overline{\mathbf{B}}^{(1)}\langle e^{-i\overline{p}_*^{(1)}\eta z}\rangle\overline{\mathbf{q}}^{(1)}\\ \tilde{\mathbf{s}}^{(1)}(y_1,y_2,z;\mathbf{d})&=-\overline{\mathbf{C}}^{(1)}\langle e^{-i\overline{p}_*^{(1)}\eta(z-d)}\rangle\overline{\mathbf{q}}^{\infty}-\overline{\mathbf{C}}^{(1)}\langle e^{-i\overline{p}_*^{(1)}\eta z}\rangle\overline{\mathbf{q}}^{(1)}.\end{aligned} \tag{7}$$

For $0\leq z<d$ (in material 1):

$$\begin{aligned}\tilde{\mathbf{u}}^{(1)}(y_1,y_2,z;\mathbf{d})&=i\eta^{-1}\mathbf{A}^{(1)}\langle e^{-ip_*^{(1)}\eta(z-d)}\rangle\mathbf{q}^{\infty}-i\eta^{-1}\overline{\mathbf{A}}^{(1)}\\ &\quad\times\langle e^{-i\overline{p}_*^{(1)}\eta z}\rangle\overline{\mathbf{q}}^{(1)}\\ \tilde{\mathbf{t}}^{(1)}(y_1,y_2,z;\mathbf{d})&=\mathbf{B}^{(1)}\langle e^{-ip_*^{(1)}\eta(z-d)}\rangle\mathbf{q}^{\infty}-\overline{\mathbf{B}}^{(1)}\langle e^{-i\overline{p}_*^{(1)}\eta z}\rangle\overline{\mathbf{q}}^{(1)}\\ \tilde{\mathbf{s}}^{(1)}(y_1,y_2,z;\mathbf{d})&=\mathbf{C}^{(1)}\langle e^{-ip_*^{(1)}\eta(z-d)}\rangle\mathbf{q}^{\infty}-\overline{\mathbf{C}}^{(1)}\langle e^{-i\overline{p}_*^{(1)}\eta z}\rangle\overline{\mathbf{q}}^{(1)}.\end{aligned} \tag{8}$$

For $z<0$ (in material 2):

$$\begin{aligned}\tilde{\mathbf{u}}^{(2)}(y_1,y_2,z;\mathbf{d})&=i\eta^{-1}\mathbf{A}^{(2)}\langle e^{-ip_*^{(2)}\eta z}\rangle\mathbf{q}^{(2)}\\ \tilde{\mathbf{t}}^{(2)}(y_1,y_2,z;\mathbf{d})&=\mathbf{B}^{(2)}\langle e^{-ip_*^{(2)}\eta z}\rangle\mathbf{q}^{(2)}\\ \tilde{\mathbf{s}}^{(2)}(y_1,y_2,z;\mathbf{d})&=\mathbf{C}^{(2)}\langle e^{-ip_*^{(2)}\eta z}\rangle\mathbf{q}^{(2)}\end{aligned} \tag{9}$$

where

$$\langle e^{-ip_*\eta z}\rangle=\mathrm{diag}[e^{-ip_1\eta z},e^{-ip_2\eta z},e^{-ip_3\eta z}] \tag{10}$$

and

$$\mathbf{q}^{\infty}=(\mathbf{A}^{(1)})^T\mathbf{f}e^{iy_\alpha d_\alpha},\quad \overline{\mathbf{q}}^{\infty}=(\overline{\mathbf{A}}^{(1)})^T\mathbf{f}e^{iy_\alpha d_\alpha}. \tag{11}$$

In Eqs. (7)–(9), p_j $(j=1,2,3)$, and $\mathbf{A}$, $\mathbf{B}$, and $\mathbf{C}$ are the Stroh eigenvalues and the corresponding eigenmatrices, and their expressions, being functions of the elastic stiffness tensor and the Fourier angular variable θ, can be found in Pan and Yuan [37]. Also in Eqs. (7)–(9), η is the Fourier radial variable defined by Eq. (6), and $\tilde{\mathbf{s}}$ the Fourier transform of the in-plane stress vector $\mathbf{s}$ defined by

$$\mathbf{s}\equiv(\sigma_{11},\sigma_{12},\sigma_{22}). \tag{12}$$

One important feature associated with the extended three-dimensional Stroh formalism is that the Stroh eigenvalues p_j and the corresponding eigenmatrices **A**, **B**, and **C** in Eqs. (7)–(9) are all independent of the Fourier radial variable η! This is actually the key in success of carrying out exactly the infinite integral with respect to the Fourier radial variable η, reducing the bimaterial Green's function to an expression in terms of a simple line integral of θ over a finite interval $[0,\pi]$ ([37]). Furthermore, as will be shown next, similar concise expression can also be obtained even for the three imperfect interface models, upon introducing certain modified eigenmatrics associated with the imperfect interface conditions.

To determine the complex vectors $\overline{\mathbf{q}}^{(1)}$ and $\mathbf{q}^{(2)}$ in Eqs. (7)–(9), one of the interface models should be applied, and they are discussed below one by one.

Model 1. For the perfect bond, we found ([37])

$$\mathbf{A}^{(1)}\langle e^{ip_*^{(1)}\eta d}\rangle\mathbf{q}^{\infty}-\overline{\mathbf{A}}^{(1)}\overline{\mathbf{q}}^{(1)}=\mathbf{A}^{(2)}\mathbf{q}^{(2)} \tag{13a}$$

$$\mathbf{B}^{(1)}\langle e^{ip_*^{(1)}\eta d}\rangle\mathbf{q}^{\infty}-\overline{\mathbf{B}}^{(1)}\overline{\mathbf{q}}^{(1)}=\mathbf{B}^{(2)}\mathbf{q}^{(2)}. \tag{13b}$$

Model 2. For the smooth bond, the interface conditions for the complex vectors $\overline{\mathbf{q}}^{(1)}$ and $\mathbf{q}^{(2)}$ are

$$\begin{pmatrix} B_{11}^{(1)} & B_{12}^{(1)} & B_{13}^{(1)} \\ B_{21}^{(1)} & B_{22}^{(1)} & B_{23}^{(1)} \\ B_{31}^{(1)} & B_{32}^{(1)} & B_{33}^{(1)} \end{pmatrix}\langle e^{ip_*^{(1)}\eta d}\rangle\mathbf{q}^{\infty}-\begin{pmatrix} \overline{B}_{11}^{(1)} & \overline{B}_{12}^{(1)} & \overline{B}_{13}^{(1)} \\ \overline{B}_{21}^{(1)} & \overline{B}_{22}^{(1)} & \overline{B}_{23}^{(1)} \\ \overline{B}_{31}^{(1)} & \overline{B}_{32}^{(1)} & \overline{B}_{33}^{(1)} \end{pmatrix}\overline{\mathbf{q}}^{(1)}$$
$$=\begin{pmatrix} -B_{11}^{(2)} & -B_{12}^{(2)} & -B_{13}^{(2)} \\ -B_{21}^{(2)} & -B_{22}^{(2)} & -B_{23}^{(2)} \\ B_{31}^{(2)} & B_{32}^{(2)} & B_{33}^{(2)} \end{pmatrix}\mathbf{q}^{(2)} \tag{14a}$$

$$(A_{31}^{(1)}\ A_{32}^{(1)}\ A_{33}^{(1)})\langle e^{ip_*^{(1)}\eta d}\rangle\mathbf{q}^{\infty}-(\overline{A}_{31}^{(1)}\ \overline{A}_{32}^{(1)}\ \overline{A}_{33}^{(1)})\overline{\mathbf{q}}^{(1)}$$
$$=(A_{31}^{(2)}\ A_{32}^{(2)}\ A_{33}^{(2)})\mathbf{q}^{(2)} \tag{14b}$$

$$(B_{31}^{(1)}\ B_{32}^{(1)}\ B_{33}^{(1)})\langle e^{ip_*^{(1)}\eta d}\rangle\mathbf{q}^{\infty}-(\overline{B}_{31}^{(1)}\ \overline{B}_{32}^{(1)}\ \overline{B}_{33}^{(1)})\overline{\mathbf{q}}^{(1)}$$
$$=(B_{31}^{(2)}\ B_{32}^{(2)}\ B_{33}^{(2)})\mathbf{q}^{(2)} \tag{14c}$$

$$\begin{pmatrix} B_{11}^{(1)} & B_{12}^{(1)} & B_{13}^{(1)} \\ B_{21}^{(1)} & B_{22}^{(1)} & B_{23}^{(1)} \end{pmatrix}\langle e^{ip_*^{(1)}\eta d}\rangle\mathbf{q}^{\infty}-\begin{pmatrix} \overline{B}_{11}^{(1)} & \overline{B}_{12}^{(1)} & \overline{B}_{13}^{(1)} \\ \overline{B}_{21}^{(1)} & \overline{B}_{22}^{(1)} & \overline{B}_{23}^{(1)} \end{pmatrix}\overline{\mathbf{q}}^{(1)}=0 \tag{14d}$$

$$\begin{pmatrix} B_{11}^{(2)} & B_{12}^{(2)} & B_{13}^{(2)} \\ B_{21}^{(2)} & B_{22}^{(2)} & B_{23}^{(2)} \end{pmatrix}\overline{\mathbf{q}}^{(2)}=0. \tag{14e}$$

It is observed that solving directly these equations for the complex vectors $\overline{\mathbf{q}}^{(1)}$ and $\mathbf{q}^{(2)}$ is very complicated. However, by performing certain simple additions and subtractions, these equations can be grouped equivalently into two matrix equations:

$$\begin{pmatrix} B_{11}^{(1)} & B_{12}^{(1)} & B_{13}^{(1)} \\ B_{21}^{(1)} & B_{22}^{(1)} & B_{23}^{(1)} \\ A_{31}^{(1)} & A_{32}^{(1)} & A_{33}^{(1)} \end{pmatrix}\langle e^{ip_*^{(1)}\eta d}\rangle\mathbf{q}^{\infty}-\begin{pmatrix} \overline{B}_{11}^{(1)} & \overline{B}_{12}^{(1)} & \overline{B}_{13}^{(1)} \\ \overline{B}_{21}^{(1)} & \overline{B}_{22}^{(1)} & \overline{B}_{23}^{(1)} \\ \overline{A}_{31}^{(1)} & \overline{A}_{32}^{(1)} & \overline{A}_{33}^{(1)} \end{pmatrix}\overline{\mathbf{q}}^{(1)}$$
$$=\begin{pmatrix} B_{11}^{(2)} & B_{12}^{(2)} & B_{13}^{(2)} \\ B_{21}^{(2)} & B_{22}^{(2)} & B_{23}^{(2)} \\ A_{31}^{(2)} & A_{32}^{(2)} & A_{33}^{(2)} \end{pmatrix}\mathbf{q}^{(2)} \tag{15a}$$

$$\begin{pmatrix} B_{11}^{(1)} & B_{12}^{(1)} & B_{13}^{(1)} \\ B_{21}^{(1)} & B_{22}^{(1)} & B_{23}^{(1)} \\ B_{31}^{(1)} & B_{32}^{(1)} & B_{33}^{(1)} \end{pmatrix}\langle e^{ip_*^{(1)}\eta d}\rangle\mathbf{q}^{\infty}-\begin{pmatrix} \overline{B}_{11}^{(1)} & \overline{B}_{12}^{(1)} & \overline{B}_{13}^{(1)} \\ \overline{B}_{21}^{(1)} & \overline{B}_{22}^{(1)} & \overline{B}_{23}^{(1)} \\ \overline{B}_{31}^{(1)} & \overline{B}_{32}^{(1)} & \overline{B}_{33}^{(1)} \end{pmatrix}\overline{\mathbf{q}}^{(1)}$$
$$=\begin{pmatrix} -B_{11}^{(2)} & -B_{12}^{(2)} & -B_{13}^{(2)} \\ -B_{21}^{(2)} & -B_{22}^{(2)} & -B_{23}^{(2)} \\ B_{31}^{(2)} & B_{32}^{(2)} & B_{33}^{(2)} \end{pmatrix}\mathbf{q}^{(2)}. \tag{15b}$$

It is very interesting that these two equations have a similar structure as that for the bimaterial Model 1 with perfectly bonded interface conditions (13*a*) and (13*b*). Therefore, the solution for the complex vectors $\overline{\mathbf{q}}^{(1)}$ and $\mathbf{q}^{(2)}$ can be found following the same procedure as for the perfect-bond interface. We further remark that this analogue method also works for other well-posed homogeneous interface conditions, as long as the displacement and traction vectors do not coupled in the same interface equation. If the displacement and traction components are mixed together in any interface condition, e.g., the spring-like model with interface displacement jump proportional to the interface traction, the infinite integral over η cannot be carried out exactly even for the two-dimensional isotropic bimaterial plane case ([17]).

Model 3. For the dislocation-like model, we have

$$\mathbf{A}^{(1)}\langle e^{ip_*^{(1)}\eta d}\rangle\mathbf{q}^{\infty}-\overline{\mathbf{A}}^{(1)}\overline{\mathbf{q}}^{(1)}=\mathbf{K}^{u}\mathbf{A}^{(2)}\mathbf{q}^{(2)} \tag{16a}$$

$$\mathbf{B}^{(1)}\langle e^{ip_*^{(1)}\eta d}\rangle\mathbf{q}^{\infty}-\overline{\mathbf{B}}^{(1)}\overline{\mathbf{q}}^{(1)}=\mathbf{B}^{(2)}\mathbf{q}^{(2)}. \tag{16b}$$

Model 4. For the force-like model, we have

$$\mathbf{A}^{(1)}\langle e^{ip_*^{(1)}\eta d}\rangle\mathbf{q}^{\infty}-\overline{\mathbf{A}}^{(1)}\overline{\mathbf{q}}^{(1)}=\mathbf{A}^{(2)}\mathbf{q}^{(2)} \tag{17a}$$

$$\mathbf{B}^{(1)}\langle e^{ip_*^{(1)}\eta d}\rangle\mathbf{q}^{\infty}-\overline{\mathbf{B}}^{(1)}\overline{\mathbf{q}}^{(1)}=\mathbf{K}^{t}\mathbf{B}^{(2)}\mathbf{q}^{(2)}. \tag{17b}$$

Since all the equations for $\overline{\mathbf{q}}^{(1)}$ and $\mathbf{q}^{(2)}$ have similar structures, the solutions for them can therefore be expressed uniformly as

$$\begin{aligned}\overline{\mathbf{q}}^{(1)}&=\mathbf{G}_1\langle e^{ip_*^{(1)}\eta d}\rangle\mathbf{q}^{\infty}\\ \mathbf{q}^{(2)}&=\mathbf{G}_2\langle e^{ip_*^{(1)}\eta d}\rangle\mathbf{q}^{\infty}.\end{aligned} \tag{18}$$

In this equation, the matrices $\mathbf{G}_1$ and $\mathbf{G}_2$ for the four different models are found to be

$$\begin{aligned}\mathbf{G}_1&=-(\overline{\hat{\mathbf{A}}^{(1)}})^{-1}(\overline{\hat{\mathbf{M}}^{(1)}}+\hat{\mathbf{M}}^{(2)})^{-1}(\hat{\mathbf{M}}^{(1)}-\hat{\mathbf{M}}^{(2)})\hat{\mathbf{A}}^{(1)}\\ \mathbf{G}_2&=(\hat{\mathbf{A}}^{(2)})^{-1}(\overline{\hat{\mathbf{M}}^{(1)}}+\hat{\mathbf{M}}^{(2)})^{-1}(\hat{\mathbf{M}}^{(1)}+\overline{\hat{\mathbf{M}}^{(1)}})\hat{\mathbf{A}}^{(1)}\end{aligned} \tag{19}$$

where $\hat{\mathbf{M}}^{(\alpha)}$ are the modified impedance tensors defined by

$$\hat{\mathbf{M}}^{(\alpha)}=-i\hat{\mathbf{B}}^{(\alpha)}(\hat{\mathbf{A}}^{(\alpha)})^{-1}\quad(\alpha=1,2) \tag{20}$$

with the modified eigenmatrices $\hat{\mathbf{A}}^{(\alpha)}$ and $\hat{\mathbf{B}}^{(\alpha)}$ being given below for the four different interface models.

Model 1. For the perfect bond ([37]),

$$\hat{\mathbf{A}}^{(\alpha)}=\mathbf{A}^{(\alpha)},\quad \hat{\mathbf{B}}^{(\alpha)}=\mathbf{B}^{(\alpha)};\quad(\alpha=1,2). \tag{21}$$

Model 2. For the smooth bond,

$$\hat{\mathbf{A}}^{(\alpha)}=\begin{pmatrix} B_{11}^{(\alpha)} & B_{12}^{(\alpha)} & B_{13}^{(\alpha)} \\ B_{21}^{(\alpha)} & B_{22}^{(\alpha)} & B_{23}^{(\alpha)} \\ A_{31}^{(\alpha)} & A_{32}^{(\alpha)} & A_{33}^{(\alpha)} \end{pmatrix};\quad(\alpha=1,2) \tag{22a}$$

$$\hat{\mathbf{B}}^{(1)}=\mathbf{B}^{(1)};\quad \hat{\mathbf{B}}^{(2)}=\begin{pmatrix} -B_{11}^{(2)} & -B_{12}^{(2)} & -B_{13}^{(2)} \\ -B_{21}^{(2)} & -B_{22}^{(2)} & -B_{23}^{(2)} \\ B_{31}^{(2)} & B_{32}^{(2)} & B_{33}^{(2)} \end{pmatrix}. \tag{22b}$$

Model 3. For the dislocation-like model,

$$\hat{\mathbf{A}}^{(1)}=\mathbf{A}^{(1)};\quad \hat{\mathbf{A}}^{(2)}=\mathbf{K}^{u}\mathbf{A}^{(2)}$$
$$\hat{\mathbf{B}}^{(\alpha)}=\mathbf{B}^{(\alpha)};\quad (\alpha=1,2). \tag{23}$$

Model 4. For the force-like model,

$$\hat{\mathbf{A}}^{(\alpha)}=\mathbf{A}^{(\alpha)};\quad (\alpha=1,2)$$
$$\hat{\mathbf{B}}^{(1)}=\mathbf{B}^{(1)};\quad \hat{\mathbf{B}}^{(2)}=\mathbf{K}^{t}\mathbf{B}^{(2)}. \tag{24}$$

Equations (7)–(9) are the bimaterial Green's displacements and stresses in the Fourier transformed domain. For the four different interface models, the complex vectors $\overline{\mathbf{q}}^{(1)}$ and $\mathbf{q}^{(2)}$ in Eqs. (7)–(9) have been derived in a unified form. With the exception of the perfect-bond interface, the bimaterial Green's functions for the three imperfect interface models are new. Similar to the perfect-bond bimaterial Green's functions ([37]), there are several important features pertained to these Green's functions. While a detailed discussion can be found in Pan and Yuan [37], we restate only one of the features closely related to the present work and add three new observations associated with the imperfect interface conditions:

1. As has been observed by Pan and Yuan [37], for the solutions in material 1 ($z>0$), the first term in Eqs. (7) and (8) is the Fourier-domain Green's function for the anisotropic full-space. The inverse of this Green's function, i.e., the physical-domain solution, has been developed by Tewary [39], Ting and Lee [40], Sales and Gray [41], and Tonon et al. [42] in an explicit form. Therefore, the Fourier inverse transform needs to be carried out only for the second term of the solutions, which is similar to the complementary part of the Mindlin solution, [38].
2. The modified eigenmatrices are introduced only for the purpose of determining the complex vectors $\overline{\mathbf{q}}^{(1)}$ and $\mathbf{q}^{(2)}$. The matrices **A**, **B**, and **C** in Eqs. (7)–(9) and later in the final expressions for the physical-domain Green's functions (Eqs. (25), (27), (28)) are the original ones and should not be altered.
3. The methodology is not restricted to the four interface models presented in this paper. The complex vectors $\overline{\mathbf{q}}^{(1)}$ and $\overline{\mathbf{q}}^{(2)}$ in Eqs. (7)–(9) for other imperfect interface models can be derived similarly by introducing the corresponding modified eigenmatrices. The only requirement is that the displacement and traction components are uncoupled in the interface conditions.
4. Under the assumption of two-dimensional deformation, the corresponding anisotropic bimaterial Green's functions in the physical domain with the three imperfect interface models can be derived analytically. This is given in the Appendix of this paper.

Bimaterial Green's Functions in the Physical Domain

Having obtained the bimaterial Green's function in the transformed domain, we now apply the inverse Fourier transform to Eqs. (7)–(9). To handle the double infinite integrals, the polar coordinate transform (6) is applied. In doing so, the infinite integral with respect to the radial variable η can be carried out exactly. Thus, the final bimaterial Green's function in the physical domain is expressed in terms of a regular line-integral over $[0,2\pi]$ in the source-free half-space, and as a sum of the homogeneous full-space Green's function and a regular line-integral over $[0,2\pi]$ in the point-force loaded half-space. Furthermore, the line integral over $[0,2\pi]$ can be reduced to $[0,\pi]$ using certain properties of the Stroh eigenvalues and the corresponding modified eigenvectors ([46,47]). The procedure is very similar to the perfect-bond interface ([37]) and one needs only to replace the matrices $\mathbf{G}_1$ and $\mathbf{G}_2$ with those corresponding to the given interface conditions. Listed below are the final physical-domain bimaterial Green's functions for the four different interface models.

Assuming that $z\neq 0$ or $d\neq 0$, the 3×3 Green's displacement tensor in material 1, with the first index for the displacement component and the second for the point-force direction, is found to be

$$\mathbf{U}^{(1)}(\mathbf{x};\mathbf{d})=\mathbf{U}^{\infty}(\mathbf{x};\mathbf{d})+\frac{1}{2\pi^2}\left[\int_0^{\pi}\overline{\mathbf{A}}^{(1)}\mathbf{G}_u^{(1)}(\mathbf{A}^{(1)})^T d\theta\right] \tag{25}$$

$$(\mathbf{G}_u^{(1)})_{ij}=\frac{(\mathbf{G}_1)_{ij}}{-\overline{p}_i^{(1)}z+p_j^{(1)}d-[(x_1-d_1)\cos\theta+(x_2-d_2)\sin\theta]}. \tag{26}$$

In Eq. (25), $\mathbf{U}^{\infty}(\mathbf{x};\mathbf{d})$ denotes the homogeneous full-space Green's displacement tensor with elastic properties of material 1 for which an explicit expression is available ([39–42]). In Eq. (26), the indices i and j take the range from 1 to 3.

Similarly, the bimaterial Green's stresses (traction and in-plane stress) in material 1 and the Green's displacements and stresses in material 2 can be derived as

$$\mathbf{T}^{(1)}(\mathbf{x};\mathbf{d})=\mathbf{T}^{\infty}(\mathbf{x};\mathbf{d})+\frac{1}{2\pi^2}\left[\int_0^{\pi}\overline{\mathbf{B}}^{(1)}\mathbf{G}_t^{(1)}(\mathbf{A}^{(1)})^T d\theta\right]$$
$$\mathbf{S}^{(1)}(\mathbf{x};\mathbf{d})=\mathbf{S}^{\infty}(\mathbf{x};\mathbf{d})+\frac{1}{2\pi^2}\left[\int_0^{\pi}\overline{\mathbf{C}}^{(1)}\mathbf{G}_t^{(1)}(\mathbf{A}^{(1)})^T d\theta\right] \tag{27}$$

$$\mathbf{U}^{(2)}(\mathbf{x};\mathbf{d})=-\frac{1}{2\pi^2}\left[\int_0^{\pi}\mathbf{A}^{(2)}\mathbf{G}_u^{(2)}(\mathbf{A}^{(1)})^T d\theta\right]$$
$$\mathbf{T}^{(2)}(\mathbf{x};\mathbf{d})=-\frac{1}{2\pi^2}\left[\int_0^{\pi}\mathbf{B}^{(2)}\mathbf{G}_t^{(2)}(\mathbf{A}^{(1)})^T d\theta\right] \tag{28}$$
$$\mathbf{S}^{(2)}(\mathbf{x};\mathbf{d})=-\frac{1}{2\pi^2}\left[\int_0^{\pi}\mathbf{C}^{(2)}\mathbf{G}_t^{(2)}(\mathbf{A}^{(1)})^T d\theta\right].$$

In Eq. (27), $\mathbf{T}^{\infty}(\mathbf{x};\mathbf{d})$ and $\mathbf{S}^{\infty}(\mathbf{x};\mathbf{d})$ denote the explicit Green's stresses in the homogeneous full-space with the elastic properties of material 1 ([42]) and

$$(\mathbf{G}_t^{(1)})_{ij}=\frac{(\mathbf{G}_1)_{ij}}{\{-\overline{p}_i^{(1)}z+p_j^{(1)}d-[(x_1-d_1)\cos\theta+(x_2-d_2)\sin\theta]\}^2} \tag{29}$$

$$(\mathbf{G}_u^{(2)})_{ij}=\frac{(\mathbf{G}_2)_{ij}}{-p_i^{(2)}z+p_j^{(1)}d-[(x_1-d_1)\cos\theta+(x_2-d_2)\sin\theta)]} \tag{30}$$

$$(\mathbf{G}_t^{(2)})_{ij}=\frac{(\mathbf{G}_2)_{ij}}{\{-p_i^{(2)}z+p_j^{(1)}d-[(x_1-d_1)\cos\theta+(x_2-d_2)\sin\theta]\}^2}. \tag{31}$$

Therefore, in material 1, the bimaterial Green's function is expressed as a sum of the explicit full-space Green's function and a complementary part in terms of a line integral over $[0,\pi]$; In material 2, the bimaterial Green's function is expressed in terms of a line integral over $[0,\pi]$ only. Although the bimaterial Green's function problem is complicated in nature, the final solution is very concise, indicating that the modified three-dimensional Stroh formalism is truly mathematically elegant and numerically powerful ([34,35]), especially when used jointly with the Mindlin's superposition method. Indeed, a direct application of the Fourier transform would require a three-dimensional integral for the full-space Green's function and four-dimensional integral for the half-space Green's function ([43]). Furthermore, with regard to these physical-domain bimaterial Green's functions (Eqs. (25), (27), and (28)), the following important observations can be made, with some of them being similar to those made in Pan and Yuan [37]:

1. For the complementary part of the solution in material 1 and the solution in material 2, the dependence of the solutions on the

field point $\mathbf{x}$ and source point $\mathbf{d}$ appears only through matrices $\mathbf{G}_u^{(1)}$, $\mathbf{G}_t^{(1)}$, $\mathbf{G}_u^{(2)}$, and $\mathbf{G}_t^{(2)}$ defined in Eqs. (26) and (29)–(31). Therefore, the derivatives of the bimaterial Green's functions with respect to either the field or source point can be exactly carried out under the integral sign. These derivatives are required in the boundary integral formulation for the internal stress and fracture analyses in bimaterial solids ([48]).

2. The integrals in Eqs. (25), (27), and (28) are regular if $z \neq 0$ or $d \neq 0$, and thus can be easily carried out by any standard numerical integral method such as the Gauss quadrature. Actually, Pan and Yang [49] have recently applied an adaptive integration version in order to calculate the perfect-bond bimaterial Green's function.

3. If $z \neq 0$ and $d = 0$, the bimaterial Green's function is still mathematically regular although some of its components may not have a direct and apparent physical meaning ([1]). However, the author ([46]) has recently given an indirect physical explanation using an equivalent relation between the Green's function due to a point force and that due to a point dislocation (or infinitesimal dislocation loop).

4. When the field and source points are both on the interface (i.e., $z = d = 0$), the bimaterial Green's function is then reduced to the interfacial Green's function. For this special case, the line integral involved in the Green's function expression becomes singular and the resulting finite-part integral needs to be handled with special approaches. A detailed study for the perfect-bond interface can be found in Pan and Yang ([49]) and a similar approach can be followed for the imperfect interface models.

Effects of Interface Conditions

The effect of different interface conditions on the displacement and stress fields was studied by Dundurs and Hetenyi [1], Mura [31], and Yu [14] for the isotropic bimaterial full-space. However, a systematic discussion on this issue has not been carried out yet, not to mention the complexity due to the general anisotropy. Based on the extended three-dimensional Stroh formalism and Mindlin's superposition method, we have found that the effect of different interface conditions on the displacement and stress fields can be studied with a unified formalism.

When studying the difference of the elastic fields due to different imperfect interface conditions relative to those with the perfect-bond interface (i.e., Model 1), it is noted that the full-space Green's function has no influence at all to this difference. It is the complementary part of the bimaterial solution that contributes to it! We also notice that it is the matrix $\mathbf{G}_1$ or $\mathbf{G}_2$ that totally controls such a difference. This is actually no surprising since when deriving the bimaterial solution, it is the complementary part that takes care of the different interface conditions, and it is the matrix $\mathbf{G}_1$ or $\mathbf{G}_2$ that directly accomplishes the task! Therefore, the difference of the displacement and stress fields due to imperfect and perfect interface conditions is directly proportional to the difference of the integral involving the matrix $\mathbf{G}_1$ or $\mathbf{G}_2$.

In the study presented below, we restrict ourselves to the case where the source point d is within the material 1 ($d > 0$) but the field point x can be anywhere in the bimaterials. Again, the difference is relative to the bimaterial Green's function solution corresponding to the perfect-bond interface (i.e., Model 1). We also mention that results for the derivatives of the displacements and stresses will not be given but can be obtained trivially.

For the field point in material 1 (i.e., $z > 0$), we found

$$\mathbf{U}^{(1)}(\mathbf{x};\mathbf{d})|_m - \mathbf{U}^{(1)}(\mathbf{x};\mathbf{d})|_1 = \frac{1}{2\pi^2}\left[\int_0^{\pi} \overline{\mathbf{A}}^{(1)} \Delta\mathbf{G}_u^{(1)} (\mathbf{A}^{(1)})^T d\theta\right] \tag{32}$$

$$\mathbf{T}^{(1)}(\mathbf{x};\mathbf{d})|_m - \mathbf{T}^{(1)}(\mathbf{x};\mathbf{d})|_1 = \frac{1}{2\pi^2}\left[\int_0^{\pi} \overline{\mathbf{B}}^{(1)} \Delta\mathbf{G}_t^{(1)} (\mathbf{A}^{(1)})^T d\theta\right] \tag{33}$$

$$\mathbf{S}^{(1)}(\mathbf{x};\mathbf{d})|_m - \mathbf{S}^{(1)}(\mathbf{x};\mathbf{d})|_1 = \frac{1}{2\pi^2}\left[\int_0^{\pi} \overline{\mathbf{C}}^{(1)} \Delta\mathbf{G}_t^{(1)} (\mathbf{A}^{(1)})^T d\theta\right]$$

where

$$(\Delta\mathbf{G}_u^{(1)})_{ij} = \frac{(\mathbf{G}_1|_m - \mathbf{G}_1|_1)_{ij}}{-\overline{p}_i^{(1)} z + p_j^{(1)} d - [(x_1 - d_1)\cos\theta + (x_2 - d_2)\sin\theta]} \tag{34}$$

$$(\Delta\mathbf{G}_t^{(1)})_{ij} = \frac{(\mathbf{G}_1|_m - \mathbf{G}_1|_1)_{ij}}{\{-\overline{p}_i^{(1)} z + p_j^{(1)} d - [(x_1 - d_1)\cos\theta + (x_2 - d_2)\sin\theta]\}^2}. \tag{35}$$

In Eqs. (32)–(35), the displacement and stress fields with a vertical line followed by subscript 1 are the bimaterial Green's functions corresponding to the perfect-bond interface (i.e., Model 1), and those by subscript m (=2, 3, and 4) correspond to the three imperfect interface models.

Similarly, for the field point in material 2 (i.e., $z < 0$), we obtained

$$\mathbf{U}^{(2)}(\mathbf{x};\mathbf{d})|_m - \mathbf{U}^{(2)}(\mathbf{x};\mathbf{d})|_1 = -\frac{1}{2\pi^2}\left[\int_0^{\pi} \mathbf{A}^{(2)} \Delta\mathbf{G}_u^{(2)} (\mathbf{A}^{(1)})^T d\theta\right]$$

$$\mathbf{T}^{(2)}(\mathbf{x};\mathbf{d})|_m - \mathbf{T}^{(2)}(\mathbf{x};\mathbf{d})|_1 = -\frac{1}{2\pi^2}\left[\int_0^{\pi} \mathbf{B}^{(2)} \Delta\mathbf{G}_t^{(2)} (\mathbf{A}^{(1)})^T d\theta\right] \tag{36}$$

$$\mathbf{S}^{(2)}(\mathbf{x};\mathbf{d})|_m - \mathbf{S}^{(2)}(\mathbf{x};\mathbf{d})|_1 = -\frac{1}{2\pi^2}\left[\int_0^{\pi} \mathbf{C}^{(2)} \Delta\mathbf{G}_t^{(2)} (\mathbf{A}^{(1)})^T d\theta\right]$$

where

$$(\Delta\mathbf{G}_u^{(2)})_{ij} = \frac{(\mathbf{G}_2|_m - \mathbf{G}_2|_1)_{ij}}{-p_i^{(2)} z + p_j^{(1)} d - [(x_1 - d_1)\cos\theta + (x_2 - d_2)\sin\theta)]} \tag{37}$$

$$(\Delta\mathbf{G}_t^{(2)})_{ij} = \frac{(\mathbf{G}_2|_m - \mathbf{G}_2|_1)_{ij}}{\{-p_i^{(2)} z + p_j^{(1)} d - [(x_1 - d_1)\cos\theta + (x_2 - d_2)\sin\theta]\}^2}. \tag{38}$$

Numerical Examples

Having derived the bimaterial Green's functions for the four different interface models, and discussed the effect of different imperfect interface conditions on the displacement and stress fields, we now present numerical examples for these bimaterial Green's functions. We first mention that the present bimaterial Green's functions have been checked with previously available solutions ([1,37]) for some special cases in isotropic and anisotropic bimaterials.

In the present examples, materials 1 and 2 are both orthotropic. Material 1 is the NASA fabric, a composite material made by stacking layers of a carbon warp-knit fabric that was stitched with Kevlar-29 thread prior to introducing 3501-6 epoxy resin ([37]). Material 2 is a graphite/epoxy composite with strong material anisotropy ([37]). In using these two materials, their principal material axes (E_1 and E_2), originally coincide with the x-y–axes, have been rotated 45 deg counterclockwise with respect to the x-axis. Thus the stiffness tensor C_{ijkl} of both materials in the structural coordinates (x,y,z) is monoclinic with symmetry plane at $z = 0$. This bimaterial full-space actually corresponds to the case III in Pan and Yuan ([37]), and the elastic stiffness in the reduced and dimensionless form for materials 1 and 2 are given, respectively, in Tables 1 and 2.

Some dimensionless Green's stress components in such a bimaterial full-space are presented in Figs. 1 to 5. In these figures, the point force of a unit magnitude is applied at $(0,0,d=1)$. The stresses are plotted at field points $(x,y,z) = (1,1,z)$ with z varying from -3 to 3.

Table 1 Elastic stiffness C_{ij} in material 1

.83514624D1	.33934624D1	.57053231D0	.0	.0	.17804512D1
	.83514624D1	.57053231D0	.0	.0	.17804512D1
		.15949776D1	.0	.0	.65283587D-2
			.605	.035	.0
				.605	.0
					.34414318D1

First, the effect of the interface matrices k_{ij}^u and k_{ij}^t (in Models 3 and 4) upon the bimaterial Green's stresses is studied. For simplicity, these interface matrices are assumed to have the same diagonal structure, i.e.,

$$\mathbf{K}^u = \mathbf{K}^t = \text{diag}[k,k,1] \tag{39}$$

where k varies from 0 and 1. Therefore, for Model 3, the normal displacement component is assumed to be continuous while the tangential components are not. Similarly, for Model 4, the normal traction component is assumed to be continuous but the shear components are not.

Shown in Figs. 1(a) and 1(b) are the variations of the dimensionless Green's stress component σ_{xx} due to a point force applied in the z-direction for Models 3 and 4, respectively. For both models, the interface parameter k in Eq. (39) takes the values of 1, 0.5, 0.1, 0.01, and 0.0001. While $k=1$ corresponds to the perfect-bond interface (i.e., Model 1), other k values are for the imperfect bond with $k=0.0001$ simulating the tangential zero-displacement and shear traction-free interfaces, respectively, for the dislocation-like and force-like models (the result for $k=0.0001$ is nearly identical to that for $k=0.000001$). It is observed from Figs. 1(a) and 1(b) that this Green's stress component is discontinuous across the interface for both models. Furthermore, it is found that for the dislocation-like model (Fig. 1(a)), the amount of discontinuity is the largest for the perfect-bond interface and decreases in general with decreasing k, reaching a final value when the tangential displacements are zero (i.e., $k=0$). For the force-like model (Fig. 1(b)), however, the amount of discontinuity is the smallest for the perfect-bond interface and increases with decreasing k, reaching a final value when the shear tractions are zero (i.e., $k=0$). Therefore, by varying the k value in the dislocation-like and force-like models, various load transfer situations across the interface can be simulated.

We now compare the stress distributions for the four models. In Figs. 2 to 5, cases 1, 2, 3, and 4 correspond to the perfect-bond, smooth-bond, dislocation-like, and force-like models, respectively. For models 3 and 4, the interface matrices k_{ij}^u and k_{ij}^t are given by Eq. (39) with k being fixed at 0.5.

The variations of the Green's stresses σ_{xx} and σ_{xy} due to a point force in the x and z-directions are shown in Figs. 2 and 3, with all of them being discontinuous across the interface. It is observed that the magnitudes of the Green's stress components due to the point force in x-direction are much larger than those due to the point force in z-direction (about four-five times). It is also clear that, locally, i.e., in the vicinity of the interface, different interface models can have a great influence on the stress distribution. Among the four models, the smooth interface model, i.e., model 2, shows the largest influence on the stress field near

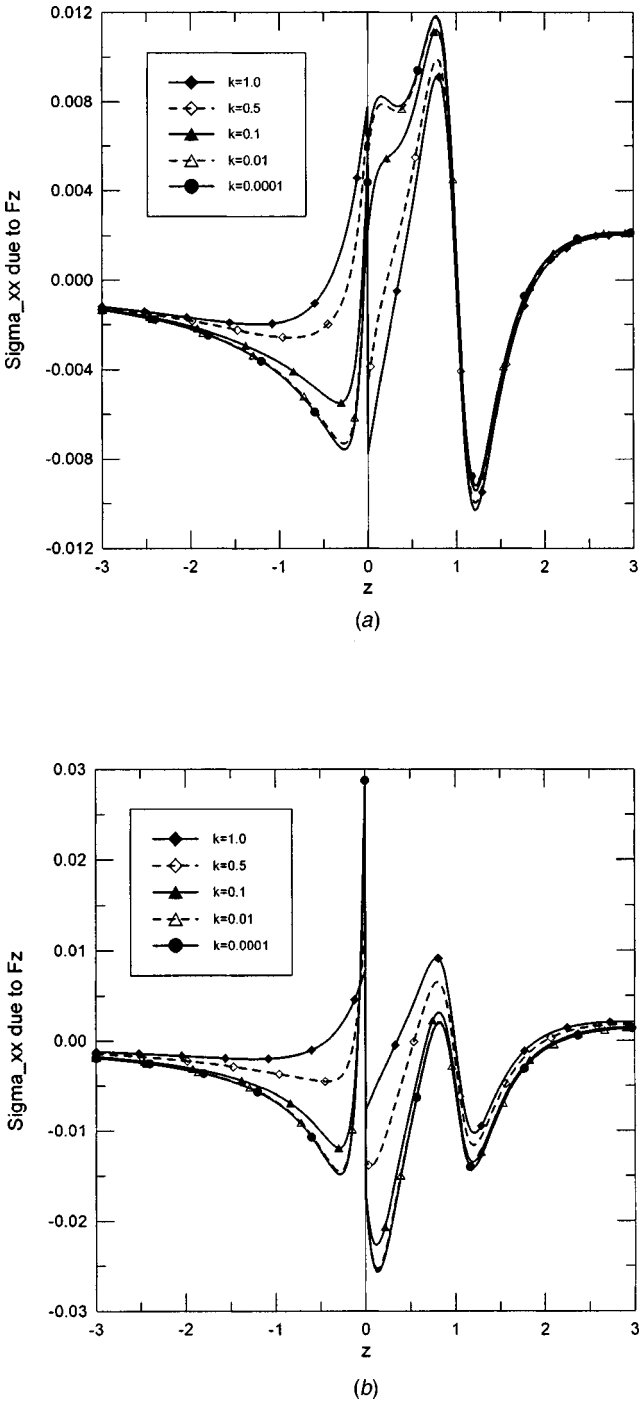

Fig. 1 Variation of the bimaterial Green's stress σ_{xx} with field point (1,1,$z\in[-3,3]$) due to a point force at d=(0,0,1) in the z-direction for different interface parameter k of dislocation-like model (*a*) and force-like model (*b*)

Table 2 Elastic stiffness C_{ij} in material 2

.71726275D1	.54524875D1	.62233525D0	.0	.0	.51191753D1
	.71726275D1	.62233525D0	.0	.0	.51191753D1
		.16217043D1	.0	.0	.11350357D0
			.64977	−.03046	.0
				.64977	.0
					.54251991D1

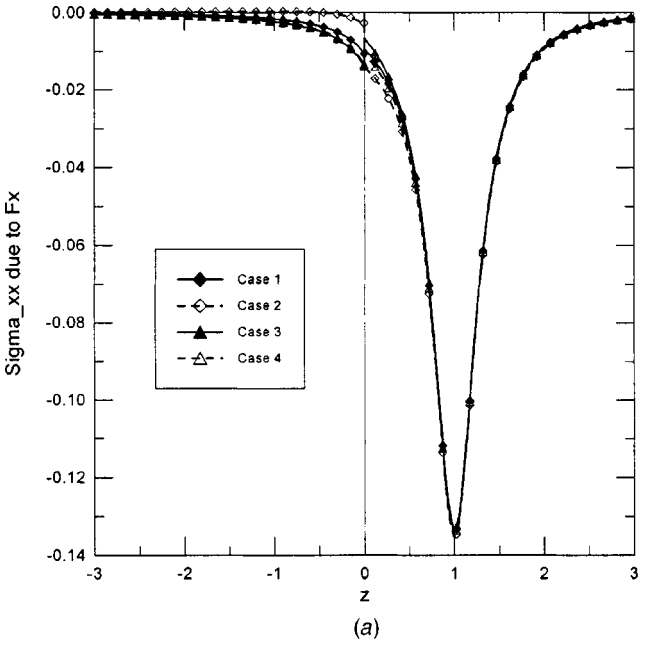

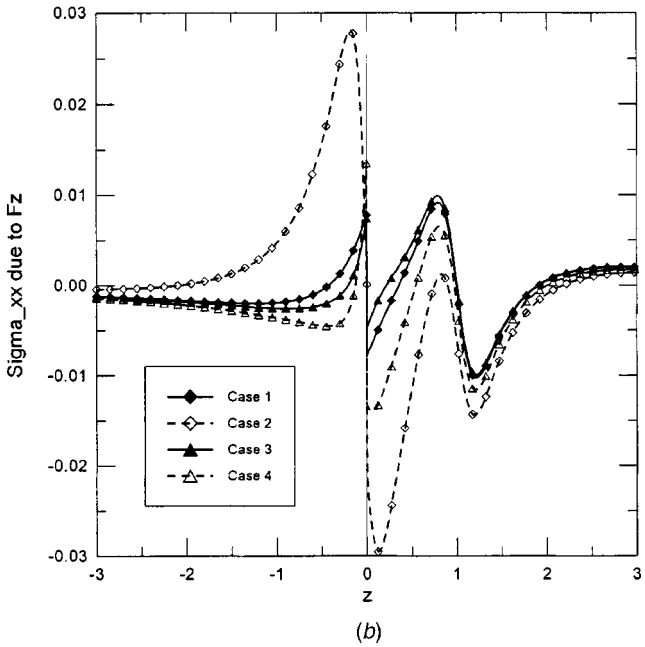

Fig. 2 Variation of the bimaterial Green's stress σ_{xx} with field point (1,1,$z\in[-3,3]$) due to a point force at d=(0,0,1) in the *x*-direction (*a*) and *z*-direction (*b*). Cases 1, 2, 3, and 4 correspond to models 1, 2, 3, and 4, respectively.

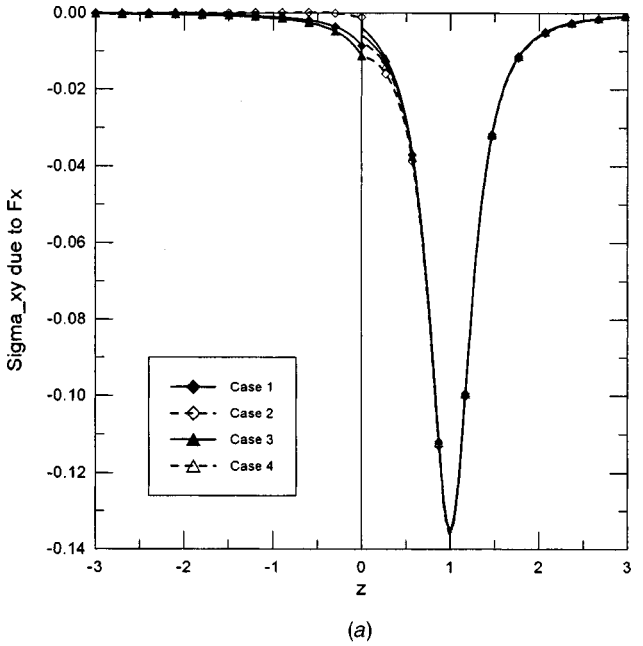

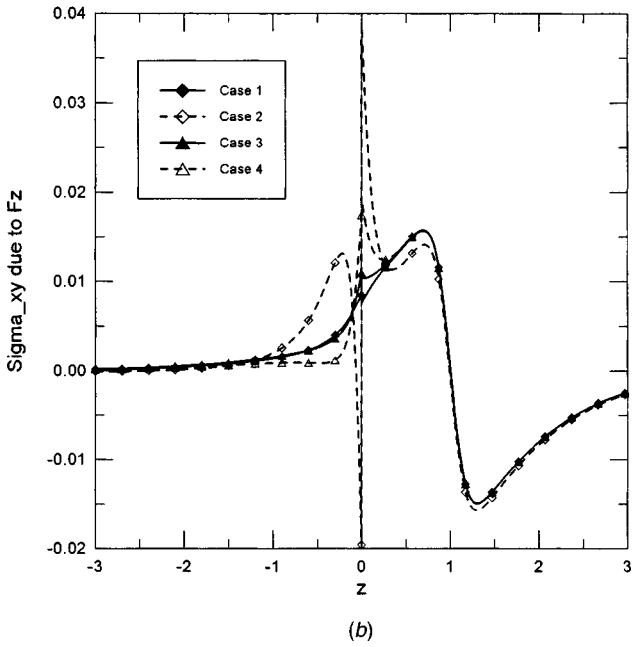

Fig. 3 Variation of the bimaterial Green's stress σ_{xy} with field point (1,1,$z\in[-3,3]$) due to a point force at d=(0,0,1) in the *x*-direction (*a*) and *z*-direction (*b*). Cases 1, 2, 3, and 4 correspond to models 1, 2, 3, and 4, respectively.

the interface. Furthermore, such an influence can be extended to a relatively far distance away from the interface, as compared to the perfect-bond model (Figs. 2(*b*) and 3(*b*)).

Shown in Figs. 4(*a*) and 4(*b*) are the variation of the shear stress σ_{xz} due to the point force in *x* and *z*-directions, respectively. For this shear stress component, its magnitudes due to the point force in *x* and *z*-directions are roughly the same. Similar to the behavior of the stresses σ_{xx} and σ_{xy}, the most affected region by the different interface models is found in the vicinity of the interface. Again, the smooth-bond model causes the greatest variation relative to the perfect-bond model. We also mention that across the interface, while σ_{xz} is continuous for models 1–3, it is discontinuous for model 4 as assumed in the model.

Finally, shown in Figs. 5(*a*) and 5(*b*) are the variations of the vertical stress σ_{zz} due to the point force in *x* and *z*-directions, respectively. For this case, the magnitude of the stress due to the point force in *z*-direction is about three times larger than that due to the point force in *x*-direction. An interesting feature is that while different interface models have nearly no effect on this stress component, the smooth-bond model, however, has a strong

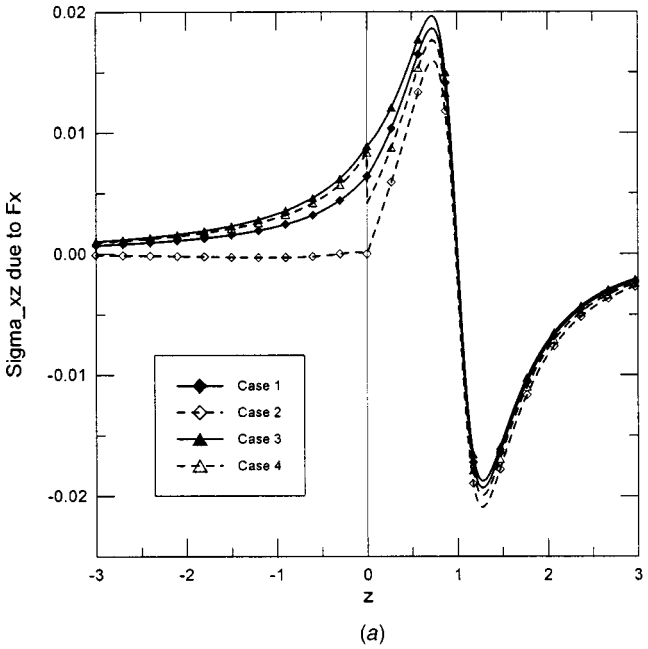

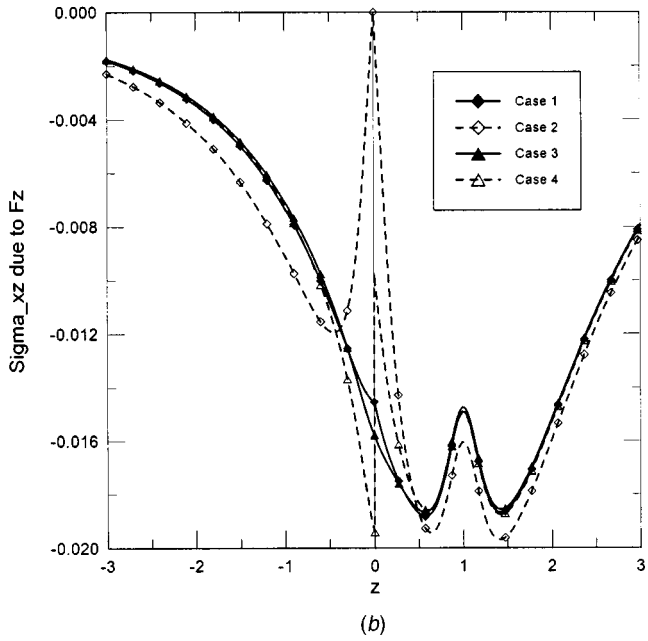

Fig. 4 Variation of the bimaterial Green's stress σ_{xz} with field point (1,1,$z\in[-3,3]$) due to a point force at d=(0,0,1) in the *x*-direction (*a*) and *z*-direction (*b*). Cases 1, 2, 3, and 4 correspond to models 1, 2, 3, and 4, respectively.

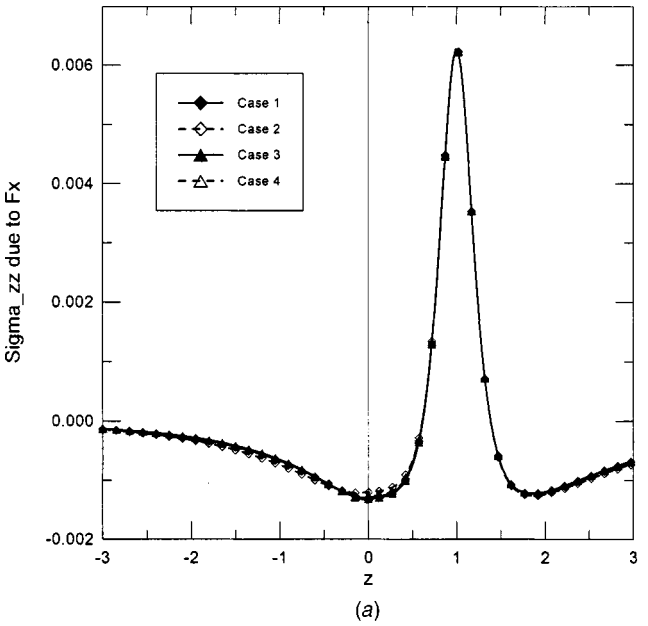

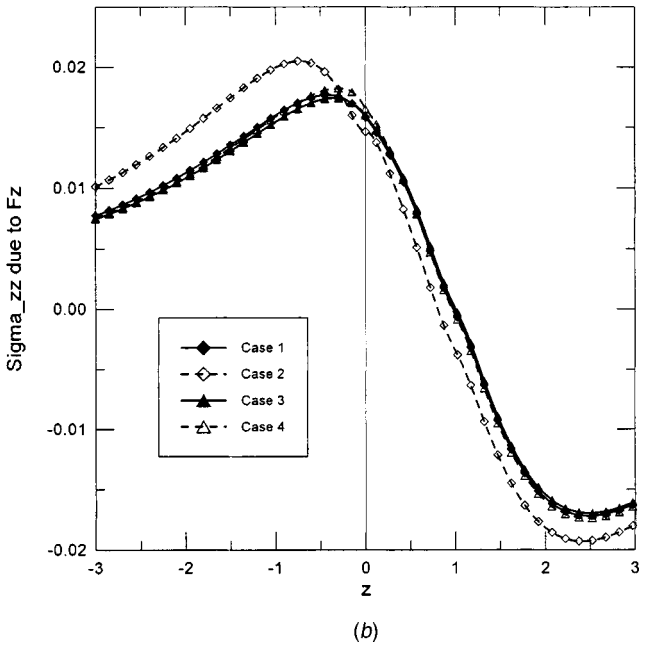

Fig. 5 Variation of the bimaterial Green's stress σ_{zz} with field point (1,1,$z\in[-3,3]$) due to a point force at d=(0,0,1) in the *x*-direction (*a*) and *z*-direction (*b*). Cases 1, 2, 3, and 4 correspond to models 1, 2, 3, and 4, respectively.

influence on this stress component when the point force is in *z*-direction. Furthermore, such an influence seems to extend to a larger region away from the interface.

Conclusions

We have derived the three-dimensional Green's functions in anisotropic bimaterials for four different interface models, namely, perfect-bond, smooth-bond, dislocation-like, and force-like. While the first model is for the perfect interface for which the corresponding bimaterial Green's functions were derived by Pan and Yuan [37], other three models are for the imperfect interface for which the corresponding bimaterial Green's functions are derived *for the first time* in this paper. A remarkable result is that for these imperfect interface models, the bimaterial Green's functions enjoy the same simple and concise structure as that for the prefect interface model. For the case of two-dimensional deformation, the corresponding bimaterial Green's functions are also derived analytically for the three imperfect interface models. We further mention that the methodology of deriving the bimaterial Green's functions with imperfect interface conditions is quite general. On the assumption that the interface displacement and traction vectors are uncoupled in the interface conditions, one needs only to construct the eigenmatrices for the given interface model in order to derive

the corresponding Green's functions. Therefore, the bimaterial Green's function corresponding to a more general interface model that combines the dislocation-like and force-like models together can be easily derived. However, it is also worthwhile to emphasize that should the interface displacement and traction vectors be coupled together, one will be unable to carry out the infinite integral over η exactly. Consequently, the bimaterial Green's function corresponding to such an interface condition would be very complicated even for the two-dimensional isotropic bimaterial case ([17]).

Numerical examples have been also carried out to study the dependence of the bimaterial Green's stresses on the interface matrices k_{ij}^u and k_{ij}^t and the effect of different interface models on the stress fields. It is observed that by varying the element values of the interface matrices k_{ij}^u and k_{ij}^t in models 3 and 4, various load transfers across the interface can be simulated. It is also shown that, among the three imperfect interface models with a middle interface value for the parameter $k(=0.5)$, the smooth-bond model shows the greatest influence on the bimaterial Green's stresses as compared to those for the perfect-bond interface. Since these bimaterial Green's functions can be obtained very efficiently and accurately, they can be easily implemented into a boundary integral formulism ([22]) to investigate the deformation, stress, and fracture problems in anisotropic and layered structures with imperfect interfaces.

Appendix

Two-Dimensional Bimaterial Green's Functions With Imperfect Interfaces. Similar to the three-dimensional bimaterial problem presented in the main text, we consider an anisotropic full-space made of two anisotropic half-spaces with interface at $z=0$. Here, however, we assume that the deformation is independent of the y-coordinate (i.e., the generalized plane-strain deformation in the (x,z) plane). We further let a line force $\mathbf{f}$ and a line dislocation with Burgers vector $\mathbf{b}$ be applied at $(x,z)=(0,d)$ with $d>0$ in material 1.

It is known that the general bimaterial Green's functions (displacements and stress functions) can be expressed as ([34,48])

$$\mathbf{u}^{(1)}=\frac{1}{\pi}\mathrm{Im}\{\mathbf{A}^{(1)}\langle\ln(z_*^{(1)}-p_*^{(1)}d)\rangle\mathbf{q}^{\infty}\}+\frac{1}{\pi}\mathrm{Im}\sum_{j=1}^{3}\{\mathbf{A}^{(1)}\langle\ln(z_*^{(1)}-\overline{p}_j^{(1)}d)\rangle\mathbf{q}_j^{(1)}\}$$
$$\boldsymbol{\phi}^{(1)}=\frac{1}{\pi}\mathrm{Im}\{\mathbf{B}^{(1)}\langle\ln(z_*^{(1)}-p_*^{(1)}d)\rangle\mathbf{q}^{\infty}\}+\frac{1}{\pi}\mathrm{Im}\sum_{j=1}^{3}\{\mathbf{B}^{(1)}\langle\ln(z_*^{(1)}-\overline{p}_j^{(1)}d)\rangle\mathbf{q}_j^{(1)}\} \tag{A1}$$

for $z>0$ (material 1), and

$$\mathbf{u}^{(2)}=\frac{1}{\pi}\mathrm{Im}\sum_{j=1}^{3}\{\mathbf{A}^{(2)}\langle\ln(z_*^{(2)}-p_j^{(1)}d)\rangle\mathbf{q}_j^{(2)}\}$$
$$\boldsymbol{\phi}^{(2)}=\frac{1}{\pi}\mathrm{Im}\sum_{j=1}^{3}\{\mathbf{B}^{(2)}\langle\ln(z_*^{(2)}-p_j^{(1)}d)\rangle\mathbf{q}_j^{(2)}\} \tag{A2}$$

for $z<0$ (material 2). In Eqs. (*A*1) and (*A*2), Im stands for the imaginary part, and the superscripts (1) and (2) denote, as in the text, the quantities in the material domain. $p_j^{(\alpha)}$ and $\mathbf{A}^{(\alpha)}$ and $\mathbf{B}^{(\alpha)}$ are the eigenvalues and the eigenmatrices similar to those given in the main text but depending upon the elastic stiffness coefficient only. Also in Eqs. (*A*1) and (*A*2),

$$\begin{aligned}\langle\ln(z_*^{(1)}-p_*^{(1)}d)\rangle&=\mathrm{diag}[\ln(z_1^{(1)}-p_1^{(1)}d),\ln(z_2^{(1)}-p_2^{(1)}d),\ln(z_3^{(1)}-p_3^{(1)}d)]\\ \langle\ln(z_*^{(1)}-\overline{p}_j^{(1)}d)\rangle&=\mathrm{diag}[\ln(z_1^{(1)}-\overline{p}_j^{(1)}d),\ln(z_2^{(1)}-\overline{p}_j^{(1)}d),\ln(z_3^{(1)}-\overline{p}_j^{(1)}d)]\\ \langle\ln(z_*^{(2)}-p_j^{(1)}d)\rangle&=\mathrm{diag}[\ln(z_1^{(2)}-p_j^{(1)}d),\ln(z_2^{(2)}-p_j^{(1)}d),\ln(z_3^{(2)}-p_j^{(1)}d)]\end{aligned} \tag{A3}$$

with the complex variable $z_j^{(\alpha)}$ being defined as

$$z_j^{(\alpha)}=x+p_j^{(\alpha)}z. \tag{A4}$$

It is seen that the first term in Eq. (*A*1) corresponds to the full-plane Green's functions (with material properties of material 1) with

$$\mathbf{q}^{\infty}=(\mathbf{A}^{(1)})^T\mathbf{f}+(\mathbf{B}^{(1)})^T\mathbf{b}. \tag{A5}$$

The second term in Eq. (*A*1) and the solution in material 2 (Eq. (*A*2)) are the complementary parts of the solution with the complex constant vectors $\mathbf{q}_j^{(\alpha)}$ $(\alpha=1,2;\ j=1,2,3)$ to be determined. For a perfect-bond interface at $z=0$, these constants are required to satisfy the following conditions ([34]) (for $j=1,2,3$):

$$\begin{aligned}\mathbf{A}^{(1)}\mathbf{q}_j^{(1)}+\overline{\mathbf{A}}^{(2)}\overline{\mathbf{q}}_j^{(2)}&=\overline{\mathbf{A}}^{(1)}\mathbf{I}_j\overline{\mathbf{q}}^{\infty}\\ \mathbf{B}^{(1)}\mathbf{q}_j^{(1)}+\overline{\mathbf{B}}^{(2)}\overline{\mathbf{q}}_j^{(2)}&=\overline{\mathbf{B}}^{(1)}\mathbf{I}_j\overline{\mathbf{q}}^{\infty}\end{aligned} \tag{A6}$$

with

$$\begin{aligned}\mathbf{I}_1&=\mathrm{diag}[1,0,0]\\ \mathbf{I}_2&=\mathrm{diag}[0,1,0]\\ \mathbf{I}_3&=\mathrm{diag}[0,0,1].\end{aligned} \tag{A7}$$

Equation (*A*6) has a similar structure as Eq. (13a,b). Therefore, the solution for the involved complex constants are found to be ([34,48])

$$\begin{aligned}\mathbf{q}_j^{(1)}&=(\mathbf{A}^{(1)})^{-1}(\mathbf{M}^{(1)}+\overline{\mathbf{M}}^{(2)})^{-1}(\overline{\mathbf{M}}^{(2)}-\overline{\mathbf{M}}^{(1)})\overline{\mathbf{A}}^{(1)}\mathbf{I}_j\overline{\mathbf{q}}^{\infty}\\ \mathbf{q}_j^{(2)}&=(\mathbf{A}^{(2)})^{-1}(\overline{\mathbf{M}}^{(1)}+\mathbf{M}^{(2)})^{-1}(\mathbf{M}^{(1)}+\overline{\mathbf{M}}^{(1)})\mathbf{A}^{(1)}\mathbf{I}_j\mathbf{q}^{\infty}\end{aligned} \tag{A8}$$

where $\mathbf{M}^{(\alpha)}$ are the impedance tensors (defined as Eq. (20)) with the eigenmatrices $\mathbf{A}$ and $\mathbf{B}$ dependent upon the material properties only.

Following the same procedure, the complex constants involved in the bimaterial Green's solutions (*A*1) and (*A*2) for the three imperfect interface models can also be determined. Similar to Eq. (*A*8), they are obtained as

$$\begin{aligned}\mathbf{q}_j^{(1)}&=(\hat{\mathbf{A}}^{(1)})^{-1}(\hat{\mathbf{M}}^{(1)}+\overline{\hat{\mathbf{M}}^{(2)}})^{-1})(\overline{\hat{\mathbf{M}}^{(2)}}-\overline{\hat{\mathbf{M}}^{(1)}})\overline{\hat{\mathbf{A}}^{(1)}}\mathbf{I}_j\overline{\mathbf{q}}^{\infty}\\ \mathbf{q}_j^{(2)}&=(\hat{\mathbf{A}}^{(2)})^{-1}(\overline{\hat{\mathbf{M}}^{(1)}}+\hat{\mathbf{M}}^{(2)})^{-1}(\hat{\mathbf{M}}^{(1)}+\overline{\hat{\mathbf{M}}^{(1)}})\hat{\mathbf{A}}^{(1)}\mathbf{I}_j\mathbf{q}^{\infty}\end{aligned} \tag{A9}$$

where $\tilde{\mathbf{M}}^{(\alpha)}$ $(\alpha=1,2)$ are the modified impedance tensors defined by Eq. (20), and the modified eigenmatrices $\hat{\mathbf{A}}^{(\alpha)}$ and $\hat{\mathbf{B}}^{(\alpha)}$ $(\alpha=1,2)$ by Eqs. (22), (23), and (24) for the three imperfect interface models. The difference between the two-dimensional and three-dimensional expressions for the modified impedance tensors and eigenmatrices is that for the two-dimensional deformation, they are functions of the elastic stiffness tensor only $(\theta=0)$; for the three-dimensional deformation, however, they depend also on the Fourier transform variable θ. We further emphasize that, for both the two-dimensional and three-dimensional deformations, the modified eigenmatrices are used only in the process of determining the involved complex constants.

With the bimaterial Green's displacements and stress functions being given by Eqs. (*A*1) and (*A*2), their derivatives with respect to the field and source points can be analytically carried out and

the resulting Green's functions can then be applied to various problems involving bimaterial plane with imperfect interfaces. As for the corresponding three-dimensional deformation, the two-dimensional bimaterial Green's functions for the three imperfect interface models have not been reported in the literature.

References

[1] Dundurs, J., and Hetenyi, M., 1965, "Transmission of Force Between Two Semi-infinite Solids," ASME J. Appl. Mech., **32**, pp. 671–674.

[2] Mura, T., and Furuhashi, R., 1984, "The Elastic Inclusion With a Sliding Interface," ASME J. Appl. Mech., **51**, pp. 308–310.

[3] Benveniste, Y., 1984, "The Effect of Mechanical Behavior of Composite Materials With Imperfect Contact Between the Constituents," Mech. Mater., **4**, pp. 197–208.

[4] Tsuchida, E., Mura, T., and Dundurs, J., 1986, "The Elastic Field of an Elliptic Inclusion With Slipping Interface," ASME J. Appl. Mech., **52**, pp. 103–108.

[5] Achenbach, J. D., and Zhu, H., 1989, "Effect of Interfacial Zone on Mechanical Behavior and Failure of Fiber-Reinforced Composites," J. Mech. Phys. Solids, **37**, pp. 381–393.

[6] Pagano, N. J., and Tandon, G. P., 1990, "Modeling of Imperfect Bonding in Fiber Reinforced Brittle Matrix," Mech. Mater., **9**, pp. 49–64.

[7] Hashin, Z., 1990, "Thermoelastic Properties of Fiber Composites With Imperfect Interface," Mech. Mater., **8**, pp. 333–348.

[8] Hashin, Z., 1991, "The Spherical Inclusion with Imperfect Interface," ASME J. Appl. Mech., **58**, pp. 444–449.

[9] Kouris, D., 1993, "Stress Concentration due to Interaction Between Two Imperfectly Bonded Fibers in a Continuous Fiber Composite," ASME J. Appl. Mech., **60**, pp. 203–206.

[10] Gao, Z., 1995, "A Circular Inclusion With Imperfect Interface: Eshelby's Tensor and Related Problems," ASME J. Appl. Mech., **62**, pp. 860–866.

[11] Hanson, M. T., and Keer, L. M., 1995, "Mechanics of Edge Effects on Frictionless Contacts," Int. J. Solids Struct., **32**, pp. 391–405.

[12] Meisner, M. J., and Kouris, D. A., 1995, "Interaction of two Elliptic Inclusions," Int. J. Solids Struct., **32**, pp. 451–466.

[13] Zhong, Z., and Meguid, S. A., 1996, "On the Eigenstrain Problem of a Spherical Inclusion With an Imperfectly Bonded Interface," ASME J. Appl. Mech., **63**, pp. 877–883.

[14] Yu, H. Y., 1998, "A New Dislocation-Like Model for Imperfect Interfaces and Their Effect on Load Transfer," Composites, **29A**, pp. 1057–1062.

[15] Yu, H. Y., Wei, Y. N., and Chiang, F. P., 2002, "Load Transfer at Imperfect Interfaces—Dislocation-Like Model," Int. J. Eng. Sci., **40**, pp. 1647–1662.

[16] Benveniste, Y., 1999, "On the Decay of End Effects in Conduction Phenomena: A Sandwich Strip With Imperfect Interfaces of Low or High Conductivity," J. Appl. Phys., **86**, pp. 1273–1279.

[17] Shilkrot, L. E., and Srolovitz, D. J., 1998, "Elastic Analysis of Finite Stiffness Bimaterial Interfaces: Application to Dislocation-Interface Interactions," Acta Mater., **46**, pp. 3063–3075.

[18] Shuvalov, A. L., and Gorkunova, A. S., 1999, "Cutting-Off Effect at Reflection-Transmission of Acoustic Waves in Anisotropic Media With Sliding-Contact Interfaces," Wave Motion, **30**, pp. 345–365.

[19] Gharpuray, V. M., Dundurs, J., and Keer, L. M., 1991, "A Crack Terminating at a Slipping Interface Between Two Materials," ASME J. Appl. Mech., **58**, pp. 960–963.

[20] Ru, C. Q., 1998, "Interface Design of Neutral Elastic Inclusions," Int. J. Solids Struct., **35**, pp. 559–572.

[21] Ru, C. Q., 1998, "A Circular Inclusion With Circumferentially Inhomogeneous Sliding Interface in Plane Elastosatics," ASME J. Appl. Mech., **65**, pp. 30–38.

[22] Pan, E., Yang, B., Cai, G., and Yuan, F. G., 2001, "Stress Analyses Around Holes in Composite Laminates Using Boundary Element Method," Eng. Anal. Boundary Elem., **25**, pp. 31–40.

[23] Vijayakumar, S., and Cormack, D. E., 1987, "Nuclei of Strain for Bi-Material Elastic Media With Sliding Interface," J. Elast., **17**, pp. 285–290.

[24] Yu, H. Y., and Sanday, S. C., 1991, "Elastic Fields in Joined Half-spaces due to Nuclei of Strain," Proc. R. Soc. London, Ser. A, **434**, pp. 503–519.

[25] Yu, H. Y., Sanday, S. C., Rath, B. B., and Chang, C. I., 1995, "Elastic Fields due to Defects in Transversely Isotropic Bimaterials," Proc. R. Soc. London, Ser. A, **449**, pp. 1–30.

[26] Davies, J. H., and Larkin, I. A., 1994, "Theory of Potential Modulation in Lateral Surface Superlattices," Phys. Rev. B, **B49**, pp. 4800–4809.

[27] Larkin, I. A., Davies, J. H., Long, A. R., and Cusco, R., 1997, "Theory of Potential Modulation in Lateral Surface Superlattices. II. Piezoelectric Effect," Phys. Rev. B, **B56**, pp. 15,242–15,251.

[28] Holy, V., Springholz, G., Pinczolits, M., and Bauer, G., 1999, "Strain Induced Vertical and Lateral Correlations in Quantum Dot Superlattices," Phys. Rev. Lett., **83**, pp. 356–359.

[29] Ru, C. Q., 1999, "Analytic Solution for Eshelby's Problem of an Inclusion of Arbitrary Shape in a Plane or Half-Plane," ASME J. Appl. Mech., **66**, pp. 315–322.

[30] Eshelby, J. D., 1957, "The Determination of the Elastic Field of an Ellipsoidal Inclusion, and Related Problems," Proc. R. Soc. London, Ser. A, **241**, pp. 376–396.

[31] Mura, T., 1987, *Micromechanics of Defects in Solids*, 2nd Ed., Martinus Nijhoff Publishers, Dordrecht, The Netherlands.

[32] Stroh, A. N., 1958, "Dislocations and Cracks in Anisotropic Elasticity," Philos. Mag., **3**, pp. 625–646.

[33] Stroh, A. N., 1962, "Steady State Problems in Anisotropic Elasticity," J. Math. Phys., **41**, pp. 77–103.

[34] Ting, T. C. T., 1996, *Anisotropic Elasticity*, Oxford University Press, Oxford, UK.

[35] Ting, T. C. T., 2000, "Recent Developments in Anisotropic Elasticity," Int. J. Solids Struct., **37**, pp. 401–409.

[36] Wu, K. C., 1998, "Generalization of the Stroh Formalism to Three-Dimensional Anisotropic Elasticity," J. Elast., **51**, pp. 213–225.

[37] Pan, E., and Yuan, F. G., 2000, "Three-Dimensional Green's Functions in Anisotropic Bimaterials," Int. J. Solids Struct., **37**, pp. 5329–5351.

[38] Mindlin, R. D., 1936, "Force at a Point in the Interior of a Semi-Infinite Solid," Physica (Amsterdam), **7**, pp. 195–202.

[39] Tewary, V. K., 1995, "Computationally Efficient Representation for Elastostatic and Elastodynamic Green's Functions," Phys. Rev. B, **51**, pp. 15,695–15,702.

[40] Ting, T. C. T., and Lee, V. G., 1997, "The Three-Dimensional Elastostatic Green's Function for General Anisotropic Linear Elastic Solids," Q. J. Mech. Appl. Math., **50**, pp. 407–426.

[41] Sales, M. A., and Gray, L. J., 1998, "Evaluation of the Anisotropic Green's Function and Its Derivatives," Comput. Struct., **69**, pp. 247–254.

[42] Tonon, F., Pan, E., and Amadei, B., 2001, "Green's Functions and BEM Formulation for 3D Anisotropic Media," Comput. Struct., **79**, pp. 469–482.

[43] Walker, K. P., 1993, "Fourier Integral Representation of the Green's Function for an Anisotropic Elastic Half-Space," Proc. R. Soc. London, Ser. A, **443**, pp. 367–389.

[44] Benveniste, Y., and Chen, T., 2001, "On the Saint-Venant Torsion of Composite Bars With Imperfect Interfaces," Proc. R. Soc. London, Ser. A, **457**, pp. 231–255.

[45] Hashin, Z., 2001, "Thin Interphase/Imperfect Interface in Conduction," J. Appl. Phys., **89**, pp. 2261–2267.

[46] Pan, E., 2003, "Three-Dimensional Green's Functions in an Anisotropic Half Space With General Boundary Conditions," ASME J. Appl. Mech., **125**, pp. 101–110.

[47] Pan, E., 2002, "Three-Dimensional Green's Functions in Anisotropic Magneto-Electro-Elastic Bimaterials," J. Appl. Math. Phys., **53**, pp. 815–838.

[48] Pan, E., and Amadei, B., 1999, "Boundary Element Analysis of Fracture Mechanics in Anisotropic Bimaterials," Eng. Anal. Boundary Elem., **23**, pp. 683–691.

[49] Pan, E., and Yang, B., 2003, "Three-Dimensional Interfacial Green's Functions in Anisotropic Bimaterials," Appl. Math. Model., in press.